Tupperwave - preliminary numerical modelling of a floating OWC equipped with a unidirectional turbine

Miguel Vicente*, Pierre Benreguig†, Sarah Crowley*, Jimmy Murphy†
*WavEC - Offshore Renewables
Rua Dom Jerónimo Osório, n^o. 11, 1^o, 1400-119 Lisboa, Portugal
E-mail:miguel.vicente@wavec.org
E-mail: sarah.crowley@wavec.org
†MaREI Centre, Beaufort Building, Environmental Research Institute, University College Cork
Ringaskiddy Co. Cork, Republic of Ireland
E-mail: pierre.benreguig@ucc.ie
E-mail: jimmy.murphy@ucc.ie

***Abstract*—The TUPPERWAVE project is supported by the European Commission's OceanEraNet program. It aims to design and validate an innovative Oscillating Water Column (OWC) Power Take-Off (PTO) concept at laboratory scale. A conventional OWC typically generates a highly fluctuating bidirectional air flow through a self-rectifying turbine. To reduce the pneumatic power fluctuations through the turbine and the acoustic impact and ultimately increase the device efficiency, the TUPPERWAVE concept generates unidirectional air flow in a closed circuit, which can be converted into electricity via a conventional, high efficiency, unidirectional turbine. The principle is based on the use of a pair of non-return valves, two additional chambers above the water column and a unidirectional turbine harnessing energy from the resulting air flow between the two chambers. The concept was adapted to a floating axisymmetric structure. Numerical time-domain models have been developed by UCC and WavEC to determine the device's primary conversion from hydrodynamic to pneumatic power. Comparison of the output from the two models showed good agreement and allowed an initial optimization of the PTO main design parameters. A set of design parameters were chosen which maximize the pneumatic average power output flowing through the turbine whilst minimizing the power fluctuations, in regular and irregular sea states. When compared to a conventional OWC with the same structure geometry, the optimised Tupperwave device was shown to produce similar pneumatic average power with much lower fluctuations.**

***Index Terms*—Wave Energy Converter, Oscillating Water Column, unidirectional turbine, numerical modelling, optimization**

I. Introduction

Climate change and its relation with global energy consumption is a topic of the utmost importance, and the need to tackle this problem is increasingly urgent. Given some estimates of the potential of ocean wave energy [1], the harvesting of this form of renewable energy may contribute to the decrease of consumption of fossil fuels.

Amongst a variety of wave energy converter (WEC) concepts, the oscillating water column (OWC) is one of the most studied and more promising. The technology has been thoroughly reviewed in several works such as in [2]. The OWC concept presents some interesting characteristics: the absence of submerged moving parts and, more importantly, the adaptability to different scenarios. The structure may be fixed or floating, and it may be designed in such a way so it better suits the water depth and the typical wavelength of a specific location, be it onshore or offshore.

The conventional OWC concept comprises a partially submerged hollow structure, with an aperture below through which sea water enters in the chamber. The alternating rise and fall of the water inside the chamber induces the compression and expansion of the air trapped above the water. The chamber is connected to the atmosphere through a system of ducts and a turbine, through which the air is then successively forced to go outwards and inwards. In turn, an electric generator converts the rotation of the turbine into electricity.

In order to deal with the fluctuating airflow, the majority of OWC prototypes are equipped with self-rectifying bidirectional turbines, such as the Wells or impulse turbines (see [3] and [4]). However, this type of turbine has a lower efficiency than conventional unidirectional turbines. Also, since the airflow changes direction every couple of a seconds, the pneumatic power fluctuations through the turbine are significant and induce difficulties in terms of control and power quality. Moreover, as the turbine is opened to the atmosphere, significant acoustic noise can be created.

More conventional unidirectional turbines have a better efficiency, but their implementation in an OWC requires a complicated system of valves and ducts [5]. Such systems have been successfully used in small devices such as navigation buoys but have so far been considered unpractical for larger scale devices where flow rates may be of the order of $100\text{m}^3/\text{s}$. The use of unidirectional turbines have been tested in different configurations, for example with twin turbines in [6], the SeaBreath [7], or the ShoreSWEC [8].

The goal of the Tupperwave project is to design and validate at laboratory level an innovative OWC concept that mitigates the aforementioned negative features of conventional OWCs equipped with self-rectifying turbines. The Tupperwave concept generates unidirectional air flow in a closed circuit, by adding two reservoirs to the conventional OWC chamber,

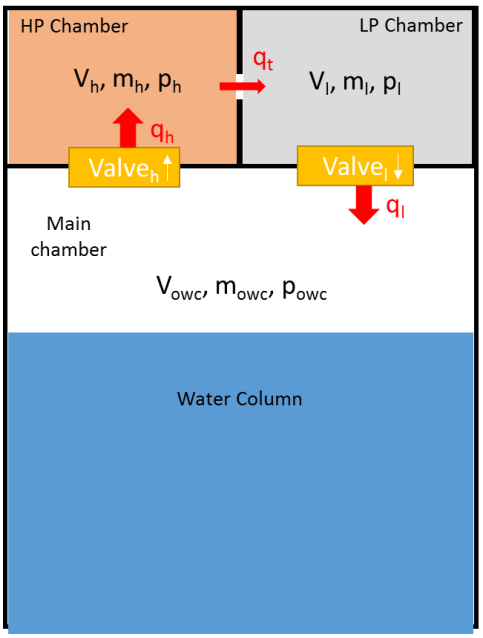

Fig. 1. Schematic diagram of the Tupperwave device concept

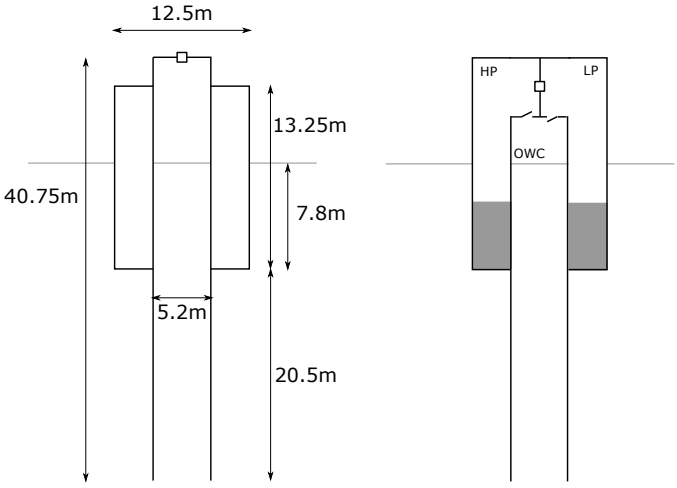

Fig. 2. Diagram of the Marinet buoy, labeled with the full-scale dimensions, and a sketch of the intended configuration of chambers within the Tupperwave concept.

a high pressure chamber and a low pressure chamber. Each of these chambers is connected with the OWC chamber through a system of non-return valves, and connected to one another by a unidirectional turbine. Fig. 1 describes schematically the working principle of the device under study.

The motion of the water column alternately pushes air into the high pressure chamber through valve h when rising, and sucks air out from the low pressure chamber through valve l when falling. The air flows rather steadily from the high to low pressure chamber across an unidirectional turbine.

This paper presents a preliminary study which consists of the development of a numerical model to simulate the device's dynamics, and its application for optimization purposes. As a reference case, it was assumed the Tupperwave concept could be integrated in a floating axisymmetric structure, with submerged dimensions based on the spar OWC developed by HMRC (now MaREI), UCC, under the Marinet project (see fig. 2). It had shown good pitching stability and therefore would provide a good support for the Tupperwave PTO system. It is assumed that the extra volume required for the additional chambers will be housed in the floater component of the buoy, see figure 2.

A time-domain model was implemented in order to understand how various design factors would affect the overall device behaviour and resulting power output. The conversion from hydrodynamic power to pneumatic power was modelled based on the linear wave theory and linearised isentropic thermodynamic equations. Only heave motion was considered, and the unidirectional valves and the turbine were modelled as a quadratic pressure drop, as if it were a simple orifice. Furthermore, it was assumed the valves completely open and close instantaneously.

A wide range of numerical simulations were carried out to test a set of design parameters, including the volumes of the three chambers, and the valve and turbine flow coefficients. Two methods to determine the radiation force were implemented by MaREI (UCC) and WavEC - the corresponding results are presented and compared. A mathematical description of the time-domain model is presented in more detail in section II. Section III presents the results of the numerical time-domain model, where simulations were run for both regular and irregular waves. Results are shown for relevant quantities, namely, the relative body and water column displacements, the air pressure within the chambers, the mass flow rate across the turbine, and the pneumatic power. The most important criteria for selecting the best configuration were considered to be a high average power, a low power fluctuation, and a reasonable maximum relative displacement value. Conclusions are summarized in section IV.

II. Model Description

In order to mathematically describe the dynamics of the Tupperwave device, several simplifications have been made. The hydrodynamic component is based on linear water wave theory, under the assumption that the body and internal free-surface motions, and the wave steepness are sufficiently small. Furthermore, in this preliminary study the thermodynamics are modelled simply as an isentropic process. The expression relating the pressure to the density is linearised, under the assumption that changes in air pressure within each of the chambers are small relative to its equilibrium value [9]. Future work will focus on improving the accuracy of the thermodynamic modelling, although it is not expected that this will have a large impact on the resulting power production predictions, see [10].

As a further simplification, only the vertical motion of the floater, also known as the heaving mode, is considered; only this mode contributes to the power conversion. Regarding the

motion of the internal water column, the approach of the generalized modes presented in [11] is adopted. The dynamic boundary condition for the chamber internal free surface is represented by a superposition of modal distributions of the vertical velocity as shown in [12]. Assuming the chamber length is small compared with the typical wavelength, it is sufficiently accurate to consider only the vertical piston-type mode. Therefore, two motion degrees of freedom have to be taken into account: the heaving mode of the floater and the vertical piston mode of the OWC.

The ordinary differential equations which drive the two degrees of freedom may be written in the following matrix form:

$$M\ddot{z} = F_{exc}\left(t\right) + F_{rad}\left(t\right) + F_{hs}\left(t\right) + F_{pto}\left(t\right) \qquad (1)$$

where M is the system's mass matrix, z is the vertical coordinate vector of the system, F_{exc} represents the excitation force inflicted by the incoming waves, F_{rad} is the hydrodynamic radiation force imposed by the motion of both the body and the water column, and F_{hs} is the hydrostatic restoring force. F_{pto} is the force induced by the power take-off equipment. No forces due to mooring lines are considered in this work.

A. Hydrodynamics

Under the linear theory, the hydrostatic restoring force is simply proportional to the amplitude of the heaving motion. The proportional factor is ρg times the respective horizontal cross section of the wetted surface. In regular waves the wave elevation profile has a sinusoidal form. The excitation force is therefore sinusoidal and frequency dependant. The hydrodynamic coefficients (added mass and hydrodynamic damping) are also frequency dependant. Excitation force and hydrodynamic coefficients were computed using the boundary element code WAMIT [13] taking into account a description of the free-surface elevation profile.

For the case of irregular waves, the excitation force is expressed as the sum of a significant set of regular waves, each with a random phase, and whose amplitude is specified by a wave spectral model.

Regarding the radiation term, it is expressed as:

$$F_{rad}\left(t\right) = A_{\infty}\ddot{z}\left(t\right) - \int_{0}^{t} K\left(t-\tau\right)\dot{z}\left(\tau\right)d\tau, \qquad (2)$$

where A_{∞} is the system's added mass at infinite frequency and K is the system impulse response function. Substituting equation (2) into the equation of motion (1), the Cummins equation is obtained [14]. The impulse response function can be calculated from the frequency dependant hydrodynamic coefficients following [15].

Two approaches were considered in this work for computing the convolution integral in eq. 2: one was to directly compute the integral at each simulation time step (MaREI, UCC). The other was to use a state-space model to approximate the convolution integral (WavEC). The convolution integral is represented by a set of first order linear differential equations using Prony's method, as explained in [16].

B. Power Take-Off component

The physical model representing Tupperwave's closed circuit, which converts the wave power to pneumatic power, is described mathematically here.

As shown in figure 1, there are three chambers: a conventional OWC chamber, a high pressure chamber (HP) and a low pressure chamber (LP), with their corresponding air pressures, p_{owc}, p_h and p_l, respectively. There are two non-return valves, valve h and valve l.

When $p_{owc} > p_h$, valve h opens and air flows from the OWC to the HP chamber through the non-return valve. Then the air is transferred through a turbine, from the HP chamber to the LP chamber. Then when $p_{owc} < p_l$, valve l opens and the air flows from the LP chamber back to the OWC chamber.

Referring to eq. 1, the term F_{pto} results from the difference in air pressure inside the OWC chamber acting upon both the internal structure of the WEC and the OWC surface:

$$F_{pto}\left(t\right) = \pm S_{owc}\left(p_{owc}\left(t\right) - p_{owc,0}\right), \qquad (3)$$

where S_{owc} is the OWC chamber cross section, p_{owc} is the instantaneous air pressure in the chamber, and $p_{owc,0}$ is its pressure in equilibrium conditions. Note that the action of the air pressure on the structure and on the OWC piston mode is the same, but with opposite signs; in the equation, the plus sign corresponds to the structure, and the minus sign to the piston mode.

In order to express the air pressure in the OWC chamber, as well as the pressure in the other two chambers (high and low pressure chambers), and ultimately the pneumatic power, the mass balance for each of the chambers is taken into account:

$$\dot{m}(t) = \frac{\partial\left(\rho(t)V(t)\right)}{\partial t} = \rho(t)\frac{\partial V(t)}{\partial t} + V(t)\frac{\partial \rho(t)}{\partial t}, \qquad (4)$$

where $\dot{m}$ is the mass flow rate for a given container, ρ is the fluid density (air, in this case), and V is the volume of the container. Assuming that the expansion/decompression of air within a given container is adiabatic and reversible, the isentropic relation can be applied

$$\frac{p}{\rho^{\gamma}} = \frac{p_{ref}}{\rho_{ref}^{\gamma}}. \qquad (5)$$

where p_{ref} and ρ_{ref} are air pressure and density in reference conditions.
Considering that the pressure and the volume of air in a given container fluctuates about an equilibrium value,

$$\begin{aligned} p(t) &= p_0 + p'(t), \\ V(t) &= V_0 + V'(t). \end{aligned} \qquad (6)$$

Using the isentropic relation in equation (5), and taking the atmospheric pressure p_0, to be the reference pressure p_{ref}, the density within the container can be written as

$$\rho = \left(1 + \frac{p'}{p_0}\right)^{\frac{1}{\gamma}} \rho_0, \qquad (7)$$

where the "(t)" notation has been suppressed. The derivative of the density ρ with respect to time is then given by

$$\frac{d\rho}{dt} = \frac{\rho_0}{\gamma}\left(\frac{p}{p_0}\right)^{\frac{1}{\gamma}-1}\frac{d}{dt}\left(\frac{p}{p_0}\right). \tag{8}$$

The mass balance within a container can then be given as:

$$\dot{m} = \rho\frac{\partial V'}{\partial t} + (V_0 + V')\frac{\partial \rho}{\partial t}, \tag{9}$$

substituting in the expression for the rate of change of the density from equation (8), it becomes

$$\dot{m} = \rho\frac{\partial V'}{\partial t} + (V_0 + V')\frac{\rho_0}{\gamma}\left(\frac{p}{p_0}\right)^{\frac{1}{\gamma}-1}\frac{d}{dt}\left(\frac{p}{p_0}\right). \tag{10}$$

This expression can be linearised, for simplification, neglecting the second order terms;

$$\begin{aligned}\dot{m} &= \rho\frac{\partial V'}{\partial t} + (V_0 + V')\frac{\rho_0}{\gamma}\left(1 + \left(\frac{1}{\gamma} - 1\right)\frac{p'}{p_0}\right)\frac{d}{dt}\left(\frac{p'}{p_0}\right) \\ &= \rho\frac{\partial V'}{\partial t} + V_0\frac{\rho_0}{\gamma}\frac{d}{dt}\left(\frac{p'}{p_0}\right).\end{aligned} \tag{11}$$

Applying equation (11) to each of the three aforementioned chambers, the following linearized expressions (12), (13), (14) may be written for the OWC chamber, the HP chamber and the LP chamber, respectively:

$$-Q_h + Q_l = -\rho_{owc}S_{owc}\frac{\partial z}{\partial t} + V_{owc0}\frac{\rho_{owc0}}{\gamma}\frac{\partial}{\partial t}\left(\frac{p_{owc}}{p_{owc0}}\right), \tag{12}$$

where Q_h is the mass flow rate from the OWC chamber to the high pressure chamber, Q_l is the mass flow rate from the low pressure chamber to the OWC chamber (both flows through the respective non-return valve), S_{owc} is the cross section area of the OWC chamber, and z_r is the relative vertical displacement between the floater and the water column inside the chamber.

$$Q_h - Q_t = V_h\frac{\rho_{h0}}{\gamma}\frac{\partial}{\partial t}\left(\frac{p_h}{p_{h0}}\right), \tag{13}$$

where Q_t is the mass flow rate across the unidirectional turbine.

$$Q_t - Q_l = V_l\frac{\rho_{l0}}{\gamma}\frac{\partial}{\partial t}\left(\frac{p_l}{p_{l0}}\right). \tag{14}$$

Subindices owc, h and l represent the OWC, the high pressure and the low pressure chambers, respectively, and the subindex 0 represents the corresponding equilibrium value (atmospheric conditions).

The non-return valves connecting the OWC chamber to each of the other chambers are not always open. They are opened only for pressure difference values above a given positive threshold. Otherwise there is no flux of air passing through. In this article, the valve are assumed to be perfect and the pressure threshold at which the valves open is 0. The valves are also assumed to be either fully opened or fully closed.

Following [17], and [18], the mass flow rate through the valves is assumed to be proportional to the square root of the pressure drop. This could be compared to an impulse or radial turbine, see for example [19]. In [17] the valve mass flow rate and is modelled via,

$$\begin{cases} Q_v = C_v L_g h_{max}\sqrt{2\rho_{air}\left(p_{up} - p_{down}\right)}, & \text{for } p_{up} > p_{down} \\ Q_v = 0 & , \text{ for } p_{up} < p_{down} \end{cases} \tag{15}$$

where C_v is the discharge coefficient for the valve, L_g is the total edge length of the valve plate and h_{max} the maximum valve opening. The pressures p_{up} and p_{down} are, respectively, the upstream and down stream pressures across the valve. [17] performs experimental tests on a model valve for which $L_g = 471.2$mm and $h_{max} = 3.14$mm. The expression used by [17] is slightly more complicated, and requires the instantaneous height of the valve opening, but here the same simplified approach of [18] is considered, which assumes that the valve is either completely open or completely closed and the mass flow rate proportional to the valve area. For a fully open valve, [17] empirically determines the discharge coefficient to be 0.69, whereas [20] uses a value of 0.5.

Hence, the mass flow rate through the valves is written:

$$\begin{cases} Q_h = C_{v,h}A_v\sqrt{2\rho_{air}\left(p_{owc} - p_h\right)}, & \text{for } p_{owc} > p_h \\ Q_h = 0 & , \text{ for } p_{owc} < p_h \end{cases} \tag{16}$$

and

$$\begin{cases} Q_l = C_{v,l}A_v\sqrt{2\rho_{air}\left(p_l - p_{owc}\right)}, & \text{for } p_l > p_{owc} \\ Q_l = 0 & , \text{ for } p_l < p_{owc} \end{cases} \tag{17}$$

where A_v is the valve surface area.

As a simplification in this preliminary analysis, similarly to the valves, the flow through the turbine is also modelled as if it were an orifice - assuming that the relationship between the mass flow rate and pressure drop is quadratic:

$$Q_t = \sqrt{\frac{p_h - p_l}{k_t}}. \tag{18}$$

Here k_t is the turbine flow coefficient, which is given by

$$k_t = \left(2\rho_{air}A^2C_t^2\right)^{-1}, \tag{19}$$

where A is the area of the orifice and C_t the discharge coefficient.

The value taken for C_t, varies but is typically between 0.5-1: [18] uses 0.6, whereas according to [20], the measured value for the discharge coefficient for a smooth venturi ranges from 0.95 to 0.97, but then went on to use a value of 0.9 in their own model. The static pressure in all of the chambers is assumed to be atmospheric.

Finally, the pneumatic power available to the turbine is

$$P_{prs} = \frac{1}{\rho_{air}}Q_t\left(p_h - p_l\right). \tag{20}$$

III. Numerical Model Results

In this section the most relevant results from the numerical model presented in the previous section are displayed. Since two approaches were used to compute the radiation term, their results first need to be compared. The results in regular

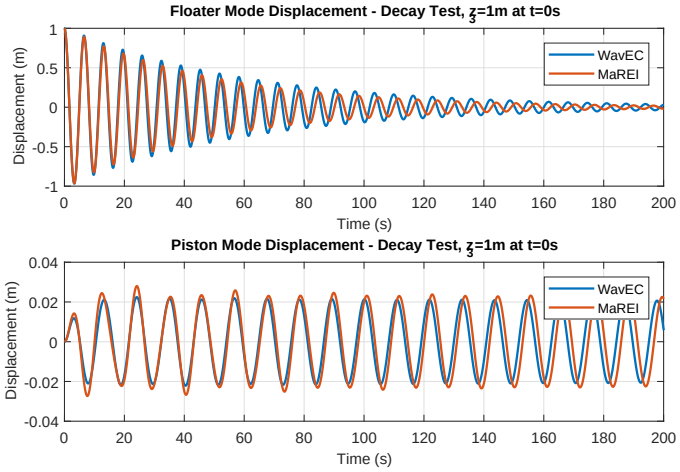

Fig. 3. Floater decay test for both methods of computing the radiation force

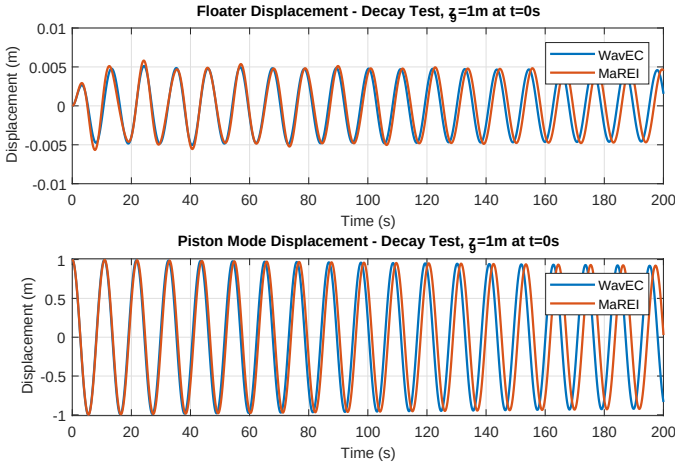

Fig. 4. Piston decay test for both methods of computing the radiation force

waves are then presented and commented. A description of the method to optimise the main design parameters follows, and finally the performance of the optimized Tupperwave device is compared against a conventional OWC device.

A. *Comparison of the two approaches for the radiation force*

Since WavEC and MaREI used two different methods to compute the convolution integrals of the radiation force (eq. 2), it is necessary to compare the results from both approaches.

A standard hydrodynamic model verification procedure is to carry out a decay test. In order to take into account only the system's hydrodynamics, the main OWC chamber is fully open to the atmosphere, and thus there is no effect from the PTO (no damping nor stiffness). The decay test is carried out in flat water - no excitation force.

Results are shown for two decay tests, one of the floater, z_3, and one of the piston mode, z_9. In the former the OWC floating structure is initially positioned 1m above its equilibrium point and is released at t=0s. The hydrostatic restoring force and gravity lead to an oscillatory motion around the equilibrium, whose amplitude is increasingly attenuated by the hydrodynamic damping, until the motion is not significant any more. The water surface also gets slightly excited by the motion of the structure.

For each body, the time interval between consecutive crests should correspond to their expected resonance period. Figure 3 and 4 shows the results of the floater and piston decay tests obtained with both models.

The displacements given by the two methods are very similar but do not overlap exactly. In figure 3 the structure's motion is more damped in MaREI's model and the water column is slightly more excited. Some difference is seen in the decay of the water column in the initial transient regime, which may become relevant in irregular waves. Despite the difference in phase that is seen in both decay tests, this leads to only a 1% difference in the expected resonance period which we consider to be within a suitable tolerance.

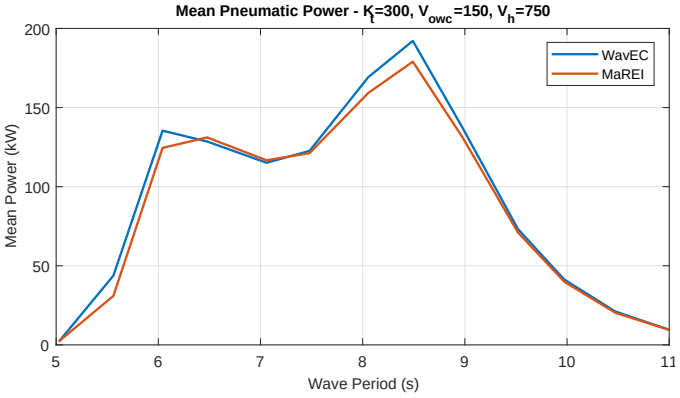

Fig. 5. Pneumatic power output of the device in 2m high regular waves assessed with both WavEC and MaREI's models

When considering the PTO, the time series in regular waves did not overlap exactly but showed good similarities. Figure 5 compares the two models results of the mean pneumatic power output in 2m high regular waves for a device equipped with a turbine damping coefficient of $k_t = 300kg^{-1}.m^{-1}$ and chambers volume of $V_{lp} = V_{hp} = 750m^3$ and $V_{owc} = 150m^3$.

The mean power output results in regular waves show good agreement. Although there are some differences in the resulting mean power predictions close to the resonant periods, both simulations show the same trends. Two main peaks are observed, corresponding to the two bodies resonance frequencies. The first peak corresponds to the spar resonance period while the second peak corresponds to the water column resonance period.

Ultimately in the remainder of this study we will be concerned with the mean power and power fluctuation averaged across wave periods. Generally for the pairs of parameters $(k_t; V_h)$ tested a difference of less than 5% was seen in these calculations. Assuming the similarity between the results of both models to be acceptable, only MaREI's results will be used hereinafter.

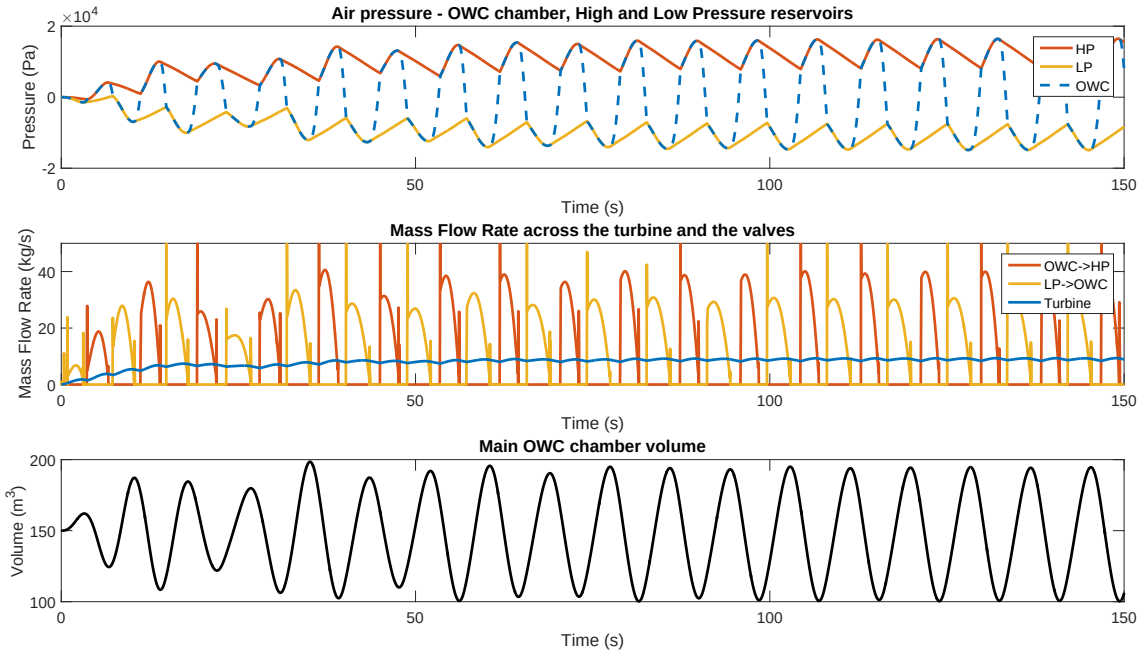

Fig. 6. 2m high Regular waves - pressures, mass flow rates and main chamber volume -series - $[V_{owc}, V_h] = [150, 750]m^3$, $k_t = 300kg^{-1}.m^{-1}$, $T = 8.5s$

B. Regular Waves Results

Figure 6 gives time series of the pressures, mass flow rates and OWC chamber volume of the Tupperwave device in a regular waves case: 2m wave height and 8.5s period.

At $t < 0s$, the device is floating on flat water and the chamber pressures are all at atmospheric pressure. At $t = 0s$ the waves start interacting with the device, and the OWC spar structure and the water column begin moving relative to each other. The volume $V_{owc}(t)$ of the main OWC chamber starts oscillating. The pressure in the HP chamber rises while the pressure in the LP chamber decreases. The mass flow rate through the turbine slowly increases. After roughly 70 seconds, $V_{owc}(t)$ follows a sinusoidal motion. The system has reached a stable regime and all variables will continue to oscillate periodically. The pressure drop between HP and LP chambers is relatively constant over time and so is the mass flow rate flowing through the turbine.

In order to fully understand what is going on in the device, a breakdown of the device working cycle is given in figure 7, which displays the pressures in the chambers and the volume of the OWC main chamber. At $t = t_1$, the main OWC chamber volume V_{owc} reduces and the pressure p_{owc} rises. Both valves are closed as $p_l < p_{owc} < p_h$. As $p_h > p_l$, chamber HP slowly discharges into chamber LP through the turbine. p_h slowly reduces while p_l slowly increases. At $t = t_2$, p_{owc} is larger than p_h. Valve h opens and air flows from the OWC chamber to the HP chamber. Since the damping induced by the opened valve is very small, the pressure drop through the opened valve is close to zero, and $p_{owc}(t) \approx p_h(t)$ during this

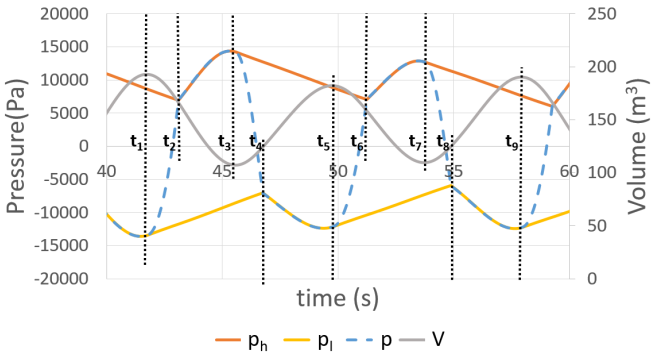

Fig. 7. Tupperwave cycle breakdown - [Vowc, Vh] = [150, 750]m3, Kt = 300kg.m, T = 8.5s

phase. As V_{owc} continues to reduce, p_h increases. At $t = t_3$, V_{owc} starts to increase. Immediately the pressure in the main OWC chamber reduces and valve h closes. Air continues to be transferred from HP chamber to the LP chamber through the turbine. Pressure p_{owc} reduces quickly until $t = t_4$ where p_{owc} reaches p_l. Valve l opens and air flows from the LP chamber into the OWC chamber. Symmetrically to the phase $t_2 < t < t_3$, the air flows easily from chamber LP into the OWC chamber as V_{owc} continues to increase and p_l reduces. At $t = t_5$, V_{owc} reverts again its evolution and starts reducing. p_{owc} rises and valve l closes. The cycle repeats then from t_5 to t_9, and so on.

Ultimately, the pressure difference between the two chambers is kept relatively constant by the PTO. The high pressure

chamber almost constantly discharges into the low pressure chamber. The airflow rate through the turbine is unidirectional and can be harnessed with a conventional unidirectional turbine. As opposed to in a conventional OWC where the mass flow stops at each period to change direction, the mass flow rate through the turbine in the Tupperwave device is relatively constant, allowing the peak to average power ratio of the PTO to be reduced.

From a more energetic point of view. The high and low pressure chambers act as accumulators. They store, under the form of pressure, the important pneumatic energy generated in half a period by the rising or falling water column and release it at a much slower pace though the turbine. Thus, the lull of pneumatic power, observed in conventional OWC, when the water column is changing direction, is almost erased.

The pneumatic power to be harnessed is therefore much smoother compared to a conventional OWC (see section III-D). A smooth power output is a great asset as it simplifies the turbine control strategy as well as the power electronic work that needs to be done before sending the power onto the grid.

C. PTO Optimization

Ideally, the pneumatic power should be as high and as smooth as possible. An optimisation process has been undertaken to maximise the power output and minimise the power fluctuation of the Tupperwave device. The parameters to be optimized are the chambers volumes, and turbine flow coefficient.

The relative computational ease with which the simulations are run on Matlab allows to use a brute force optimisation method. The valve flow coefficients were desirably small. Both chambers HP and LP were assumed to have the same volume V_h. The tested chambers volumes are constrained by the total volume of the floater. Different values for the PTO damping k_t and for the chambers volumes V_{owc} and V_h were tested.

As explained in section II, the turbine is modelled as a quadratic pressure drop, which would compare to an orifice plate. In order to provide the reader a better idea of the tested damping coefficients, table I gives the damping coefficient k_t for different orifice diameters with a discharge coefficient C=0.74 [21].

TABLE I
DIAMETER AND THEORETICAL DAMPING OF CHAMFERED ORIFICES WITH C=0.74.

orifice diameter [cm]	Surface orifice $[m^2]$	k_t $[kg^{-1}.m^{-1}]$
59.0	0.273	10
46.9	0.173	25
39.4	0.122	50
33.1	0.0863	100
30.0	0.0705	150
25.2	0.0498	300
20.0	0.0315	750
15.0	0.0177	2386

The optimisation criteria was to maximize the power output and power smoothing. In order to characterise the power smoothing an additional variable called power fluctuation f_p was used:

$$f_p = \frac{std(P)}{\bar{P}} = \frac{1}{\bar{P}} \cdot \sqrt{\left(\frac{1}{t_{final}} \int_0^{t_{final}} \left(P(t) - \bar{P} \right)^2 dt \right)} \tag{21}$$

Optimising the smoothing is equivalent to minimizing the power fluctuation around the mean power value.

TABLE II
AVERAGE POWER OUTPUT IN 2M HIGH REGULAR WAVES FOR PERIOD FROM 5 TO 11S

Power [kW]

V_h $[m^3]$ \ k_t $[kg^{-1}.m^{-1}]$	10	25	50	100	150	**300**	**750**	2386
300	49.9	64.6	72.3	78.5	82.1	87.3	89.6	79.0
400	50.7	61.7	70.7	78.2	82.1	87.7	90.3	79.5
500	51.4	61.0	69.4	77.6	81.8	87.8	90.5	79.6
750	49.7	59.2	67.4	76.1	80.9	87.4	90.5	79.4
950	49.0	58.0	66.2	80.2	83.8	90.0	90.2	78.8
1000	48.8	57.7	66.0	75.1	80.0	87.0	90.1	78.7

TABLE III
AVERAGE POWER FLUCTUATION TABLE IN 2M HIGH REGULAR WAVES FOR PERIOD FROM 5 TO 11S

Fluctuation [%]

V_h $[m^3]$ \ k_t $[kg^{-1}.m^{-1}]$	10	25	50	100	150	**300**	**750**	2386
300	84.9	71.0	57.5	44.8	38.0	27.9	18.3	10.9
400	80.3	63.3	49.4	36.8	30.3	21.6	13.9	8.3
500	75.1	57.5	43.3	30.9	25.1	17.5	11.2	6.8
750	66.6	46.5	32.4	21.7	17.3	11.9	7.6	5.3
950	60.6	40.0	26.7	13.8	11.4	7.3	6.1	4.8
1000	59.4	38.6	25.6	16.7	13.1	9.0	5.8	4.8

Due to the large number of test cases, results here presented are limited to the most relevant. Although not explicitly displayed, one outcome of the simulations was that V_{owc} should be small compared with V_h. The following results correspond to $V_{owc} = 150m^3$.

Focussing on the HP and LP volume and on the turbine flow coefficient, each pair $(k_t; V_h)$ was simulated in two meter high regular waves for periods ranging from 5 to 12 seconds. The simulation time was 250 seconds, but the relevant quantities are computed only for the stable regime, which is assumed to be reached after 100 seconds. Double entry tables displaying the average power and the power fluctuation are then generated to visually identify the optimum $(k_t; V_h)$ couple.

In order to choose a pair of parameters $(k_t; V_h)$ which gave a high but also broadbanded response, the power output and the power fluctuation were averaged over the wave periods 5-11s for each configuration. Results obtained in 2m high waves are displayed in tables II and III. The colour formatting allows the higher power and lower power fluctuation results to be clearly seen. The green areas in tables II and table III show the higher power and the lower power fluctuation, respectively. Highlighted in bold are the values of k_t and V_h which combine to give high power output and low fluctuation.

Table III clearly shows that $V_h = 950m^3$ provides the best power smoothness for the range of k_t highlighted. Table II shows that the average power extraction of the device

TABLE IV
AVERAGE MEAN PNEUMATIC POWER PER WAVE HEIGHT SQUARED AND AVERAGE POWER FLUCTUATION ACROSS WAVE PERIODS T=5-11S FOR $[k_t = 300kg^{-1}.m^{-1}; V_h = 950m^3]$ FOR WAVE HEIGHTS H=1,2, AND 4M.

Wave height [m]	H=1 [m]	H=2 [m]	H=4 [m]
Average mean power [kW/m^2]	20.13	21.77	21.99
Average power fluctuation [-]	13.69	9.43	6.71

in regular waves depends on the damping coefficient more than the chamber volume. In general, the power fluctuations decrease as the damping coefficient and chamber volume increase.

Numerical simulations in 1m and 4m high waves showed that the optimized turbine damping value k_t decreases as the wave height increases, whereas the ideal chamber volume was invariant to wave height. Table IV gives the average mean pneumatic power per wave height squared and average power fluctuation across wave periods T=5-11s for the configuration $[k_t = 300kg^{-1}.m^{-1}; V_h = 950m^3]$ for wave heights H=1,2, and 4m. The average mean pneumatic power is shown to increase in proportion to the wave height squared, whereas the power fluctuation decreases as the wave height increases.

The optimal PTO damping depends on the sea state and needs to be tuned accordingly [22]. In the case of an actual unidirectional PTO turbine, the damping can be tuned by controlling the turbine rotational speed or the pitching of the blades. Similarly to conventional OWC devices, it was observed that, for a given wave height higher PTO damping gives better power output in longer period waves while lower PTO damping gives more power in shorter period waves. For 2m high waves, the value $k_t = 300kg^{-1}.m^{-1}$ provides similar amounts of mean power for wave periods from 6 to 9 seconds as will be observed in the next section (figure 8).

The PTO configurations $[k_t = 300 - 750kg^{-1}.m^{-1}; V_h = 750 - 950m^3]$ provide on average the highest power output and lowest power fluctuation relative to all values tested in the regular wave simulations in 1 to 4m high waves across wave periods from 5 to 11s. A visualisation of the $[V_h = 750m^3]$ configuration with full scale measurements is shown in Figure 12.

D. Performance comparison with conventional OWC

In parallel to the modelling of the Tupperwave device, a conventional OWC was modelled using the same OWC spar structure. The bidirectional PTO turbine was also modelled by a quadratic pressure drop. The damping was optimised to maximize the power output using the same brute force method described in the previous section. The optimized damping coefficient for the conventional OWC in 2m high regular waves was $k_t = 25kg^{-1}.m^{-1}$, and results are compared with the $[k_t = 300kg^{-1}.m^{-1}; V_h = 950m^3]$ Tupperwave configuration. Note that the PTO damping required in the Tupperwave device is higher than for the conventional OWC.

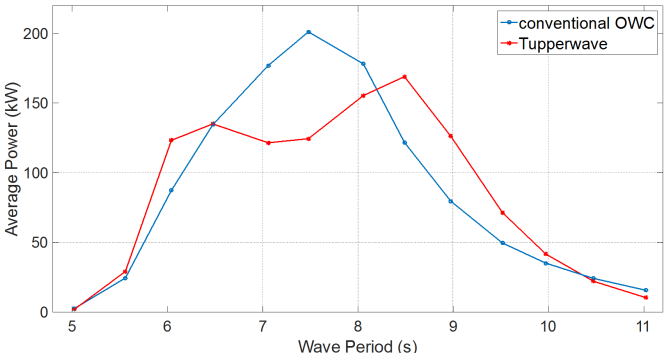

Fig. 8. Pneumatic Power in 2 meter high regular waves for conventional OWC and optimized Tupperwave device

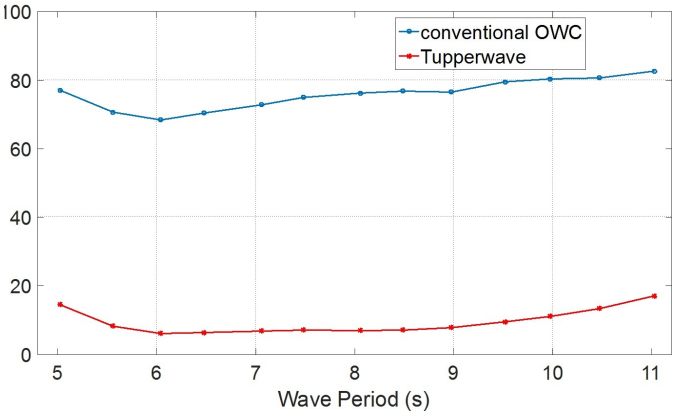

Fig. 9. Power fluctuation in 2 meter high regular waves for conventional OWC and optimized Tupperwave device

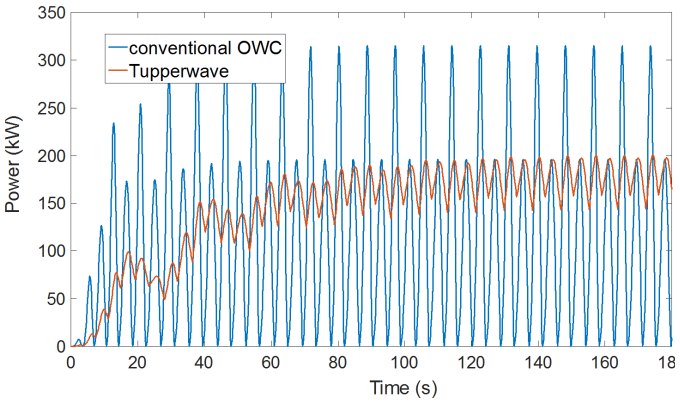

Fig. 10. Pneumatic power generation by Tupperwave device $\{[Vowc, Vh] = [150, 750]m^3, k_t = 300kg^{-1}.m^{-1}\}$ and conventional OWC device $\{k_t = 25kg^{-1}.m^{-1}\}$ in 2m high regular waves of period $T = 8.5s$

Figure 8 and 9 compare the power and power fluctuation curves of the conventional OWC and the Tupperwave device. While the power outputs of the two devices are of similar order, the power fluctuation is 8 times smaller for the Tupperwave device. The Tupperwave device delivers a better power

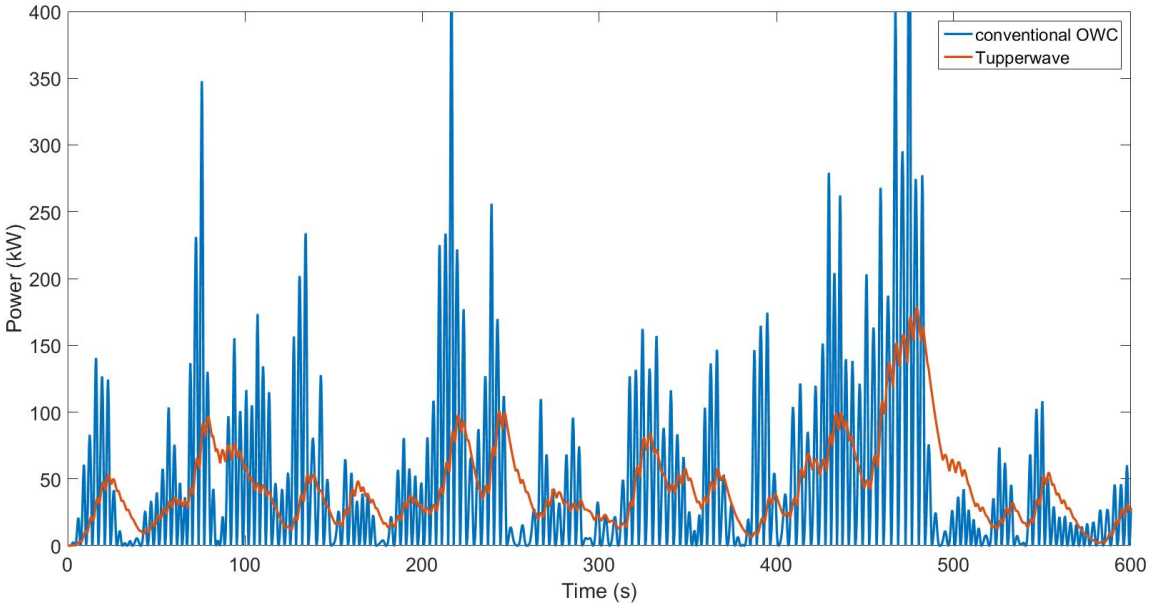

Fig. 11. Pneumatic power generation by Tupperwave device $\{[Vowc, Vh] = [150, 950]m^3, k_t = 750kg^{-1}.m^{-1}\}$ and conventional OWC device $\{k_t = 25kg^{-1}.m^{-1}\}$ in 2m significant height irregular waves of period $T = 8s$

quality than the conventional OWC modelled here. It should be noted however that, in practice typical OWC turbines have a flywheel mechanism (not modelled here), which helps with the smoothing of the power. The results are indicative however, that the Tupperwave PTO allows for smoothing similar to that which a flywheel would usually provide.

To illustrate the difference in power quality, figure 10 displays the power time series of the conventional OWC and the Tupperwave device in 2 meter high regular waves of 8.5s period. While the conventional OWC power oscillates between 0 and its highest peaks every half-period, the Tupperwave instantaneous power shows smaller oscillations. For this wave period, the Tupperwave device also shows a higher average power than the conventional OWC once the stable regime is reached as shown in figure 8.

Figure 11 displays the power time series of the conventional OWC and the Tupperwave device in irregular sea state of Hs=2m and Tp=8s. The pneumatic power across the Tupperwave PTO is not only smoothed in-between wave periods but also in-between the wave groups.

In regular waves the Tupperwave device has a capture width ratio greater than 0.3 across wave periods from 6-9s, with a maximum of 0.45. Although ideally a mean capture width ratio would be calculated using a power matrix and a scatter plot for a particular site, here we make a simple rough approximation. Taking a non-weighted average of the capture width ratio across wave periods from 5-11s results in a mean capture width ratio close to 25% which falls within the range reported in [23] typically expected of OWC concepts.

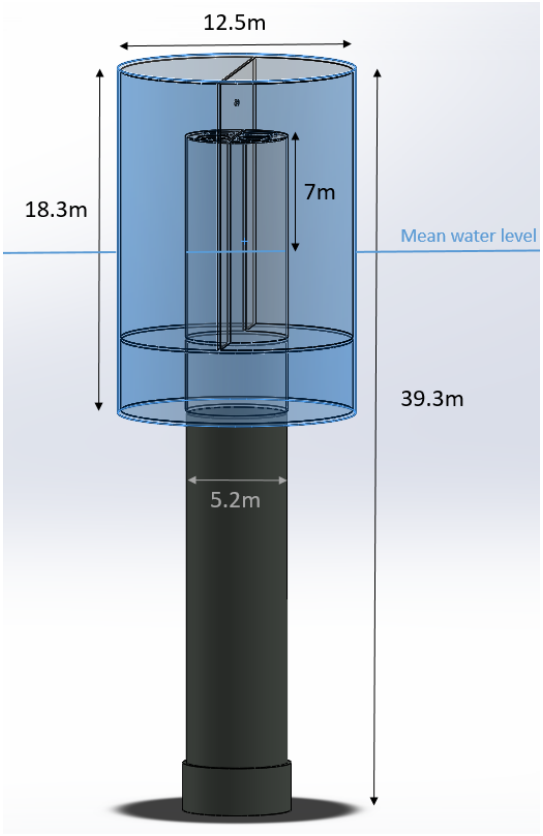

Fig. 12. Solidworks design of the optimised Tupperwave device

IV. Conclusions

This paper presented the innovative Tupperwave OWC concept adapted to a floating spar type OWC structure and a numerical model to assess its performance. An optimisation of the Tupperwave PTO main parameters has been performed to maximise the average pneumatic power output and minimize the power fluctuations in regular waves. Once optimised, the Tupperwave device performed well, both in regular and in irregular waves, particularly regarding the power fluctuation criterion. The Tupperwave device has a much lower power fluctuation when compared with the highly fluctuating bidirectional air flow of the conventional OWC, corresponding to a higher pneumatic power quality. The efficiency of unidirectional turbines being higher than self rectifying turbines, more pneumatic power is expected to be converted into electrical power. Also, due to the low power fluctuations, the Tupperwave concept might require a less complex turbine control system and could utilise more efficient power electronics equipment.

Despite some assumptions that simplify the numerical model, the results look physically acceptable. Nevertheless, future work within the Tupperwave project will be focussed on improving the thermodynamics modelling, and characterizing the unidirectional turbine. CFD simulations are currently being carried out under the Tupperwave project by CADFEM Ireland. Their results will be compared to the numerical results presented in this article. The device will also be tested at small scale in the LIR National Ocean Test Facility in Cork in summer 2017, which will be an opportunity to validate the numerical model.

Acknowledgment

The authors would like to acknowledge funding received through OCEANERA-NET European Network (OCN/00028).

References

[1] G. Mork, S. Barstow, A. Kabuth, and M. T. Pontes, "Assessing the global wave energy potential," in *29th International Conference on Ocean, Offshore and Arctic Engineering: Volume 3. ASME, pp. 447454*. OMAE 2010, 2010.

[2] A. F. Falcão and J. C. Henriques, "Oscillating-water-column wave energy converters and air turbines: A review," *Renewable Energy*, vol. 85, pp. 1391–1424, 2016.

[3] S. Raghunathan, "The wells air turbine for wave energy conversion," *Prog. Aerosp. Sci.*, vol. 31, pp. 335–386, 1995.

[4] B. Pereiras, F. Castro, A. El Marjani, and M. A. Rodríguez, "An improved radial impulse turbine for owc," *Renewable Energy*, vol. 36, no. 5, pp. 1477–1484, 2011.

[5] Y. Masuda and T. Miyazaki, "Wave power electric generation study in japan," in *International Symposium on Wave and Tidal Energy*, vol. 1, 1978, p. 6.

[6] V. Jayashankar, S. Anand, T. Geetha, S. Santhakumar, V. J. Kumar, M. Ravindran, T. Setoguchi, M. Takao, K. Toyota, and S. Nagata, "A twin unidirectional impulse turbine topology for owc based wave energy plants," *Renewable Energy*, vol. 34(3), pp. 692–698, 2009.

[7] L. Martinelli, P. Pezzutto, and P. Ruol, "Experimentally based model to size the geometry of a new owc device, with reference to the mediterranean sea wave environment," *Energies*, vol. 6(9), p. 46964720, 2013.

[8] J. R. Joubert, "Design and development of a novel wave energy converter," Ph.D. dissertation, Stellenbosch University, 2013.

[9] W. Sheng, R. Alcorn, and A. Lewis, "Assessment of primary energy conversions of oscillating water columns. ii. power take-off and validations," *Journal of Renewable and Sustainable Energy*, vol. 6, 2014.

[10] A. F. Falcão and P. Justino, "Owc wave energy devices with air flow control," *Ocean Engineering*, vol. 26, no. 12, pp. 1275–1295, 1999.

[11] C.-H. Lee, J. Newman, and F. Nielson, "Wave interactions with an oscillating water column," in *Proc. of the 6th Int. Offshore and Polar Engineering Conference*, 1996.

[12] J. Lighthill, "Two-dimensional analyses related to wave-energy extraction by submerged resonant ducts." *J. of Fluid Mechanics*, vol. 91, pp. 253–317, 1979.

[13] C.-H. Lee, *WAMIT theory manual*. Massachusetts Institute of Technology, 1995.

[14] W. Cummins, "The impulse response function and ship motions," DTIC Document, Tech. Rep., 1962.

[15] T. F. Ogilvie, "Recent progress toward the understanding and prediction of ship motions," in *5th Symposium on naval hydrodynamics*, vol. 1, no. 2. Bergen, Norway, 1964, pp. 2–5.

[16] Z. Yu and J. Falnes, "State-space modelling of a vertical cylinder in heave," *Applied Ocean Research*, vol. 17, no. 5, pp. 265–275, 1995.

[17] R. A. Habing, "Flow and plate motion in compressor valves," Ph.D. dissertation, University of Twente, 2005.

[18] T. Kelly, T. Dooley, J. Campbell, and J. Ringwood, "Efforts towards a validated time-domain model of an oscillating water column with control components," in *Proceedings of the 11th European Wave and Tidal Energy Conference*, 2015.

[19] L. Gato, A. Falcão, E. Nunes, J. Henriques, and C. Rodrigues, "Model testing of a novel radial self-rectifying air turbine for use in owc wave energy converters," in *Proc. 4th International Conference on Ocean Energy*, 2012, pp. 17–19.

[20] T. Kelly, T. Dooley, J. Campbell, and J. V. Ringwood, "Comparison of the experimental and numerical results of modelling a 32-oscillating water column (OWC), v-shaped floating wave energy converter," *Energies*, vol. 6, no. 8, pp. 4045–4077, 2013.

[21] P. Benreguig, F. Thiebaut, and J. Murphy, "Pneumatic orifice calibration, investigation into the influence of test rig characteritics on calibration results," *CORE Conference, Glasgow*, 2016.

[22] W. Sheng and A. Lewis, "Power takeoff optimization to maximize wave energy conversions for oscillating water column devices," *IEEE Journal of Oceanic Engineering*, 2017.

[23] A. Babarit, "A database of capture width ratio of wave energy converters," *Renewable Energy*, vol. 80, pp. 610–628, 2015.